2015

Motor imagery classification using sparse representation of EEG signals

Pouria Saidi
University of Central Florida

MOTOR IMAGERY CLASSIFICATION USING SPARSE REPRESENTATION OF EEG SIGNALS

by

POURIA SAIDI
B.S. Shahid Bahonar University of Kerman, 2009
M.S. Amirkabir University of Technology (Tehran Polytechnic), 2012

A thesis submitted in partial fulfillment of the requirements
for the degree of Master of Science
in the Department of Electrical Engineering and Computer Science
in the College of Engineering and Computer Science
at University of Central Florida
Orlando, Florida

Summer Term
2015

Major Professor:
George Atia

ABSTRACT

The human brain is unquestionably the most complex organ of the body as it controls and processes its movement and senses. A healthy brain is able to generate responses to the signals it receives, and transmit messages to the body. Some neural disorders can impair the communication between the brain and the body preventing the transmission of these messages. Brain Computer Interfaces (BCIs) are devices that hold immense potential to assist patients with such disorders by analyzing brain signals, translating and classifying various brain responses, and relaying them to external devices and potentially back to the body.

Classifying motor imagery brain signals where the signals are obtained based on *imagined* movement of the limbs is a major, yet very challenging, step in developing Brain Computer Interfaces (BCIs). Of primary importance is to use less data and computationally efficient algorithms to support real-time BCI. To this end, in this thesis we explore and develop algorithms that exploit the sparse characteristics of EEGs to classify these signals. Different feature vectors are extracted from EEG trials recorded by electrodes placed on the scalp.

In this thesis, features from a small spatial region are approximated by a sparse linear combination of few atoms from a multi-class dictionary constructed from the features of the EEG training signals for each class. This is used to classify the signals based on the pattern of their sparse representation using a minimum-residual decision rule.

We first attempt to use all the available electrodes to verify the effectiveness of the proposed methods. To support real time BCI, the electrodes are reduced to those near the sensorimotor cortex which are believed to be crucial for motor preparation and imagination.

In a second approach, we try to incorporate the effect of spatial correlation across the neighboring electrodes near the sensorimotor cortex. To this end, instead of considering one feature vector at a time, we use a collection of feature vectors simultaneously to find the joint sparse representation of these vectors. Although we were not able to see much improvement with respect to the first approach, we envision that such improvements could be achieved using more refined models that can be subject of future works.

The performance of the proposed approaches is evaluated using different features, including wavelet coefficients, energy of the signals in different frequency sub-bands, and also entropy of the signals. The results obtained from real data demonstrate that the combination of energy and entropy features enable efficient classification of motor

imagery EEG trials related to hand and foot movements. This underscores the relevance of the energies and their distribution in different frequency sub-bands for classifying movement-specific EEG patterns in agreement with the existence of different levels within the alpha band. The proposed approach is also shown to outperform the state-of-the-art algorithm that uses feature vectors obtained from energies of multiple spatial projections.

ACKNOWLEDGMENTS

I would like to thank my esteemed advisor Dr. George Atia, for his guidance, enthusiasm mentoring and patience that have been very helpful to accomplish this research. I also want to thank my thesis committee members, Dr. Azadeh Vosoughi, Dr. Stephen Berman for spending their time to review the manuscript and providing valuable suggestions.

Finally I am indebted to and my deepest gratitude goes to my mother and father for their never-ending encouragement, support and assistance throughout my education.

TABLE OF CONTENTS

LIST OF FIGURES

LIST OF TABLES

LIST OF ACRONYMS

Band Pass Filter	BPF
Brain Computer Interface	BCI
Central Nervous System	CNS
Common Spatial Patterns	CSP
Cortical Activity	CA
Discrete Wavelet Transform	DWT
Electrocorticogram	ECoG
Electroencephalogram	EEG
Electromyogram	EMG
Electro-oculogram	EOG
Event-Related Desynchronization	ERD
Event-Related Potentials	ERP
Event-Related synchronization	ERS
functional Magnetic Resonance Imaging	fMRI
Linear Discriminant Analysis	LDA
Motor Imagery	MI
Orthogonal Matching Pursuit	OMP
Signal to Noise Ratio	SNR

Simultaneous Orthogonal Matching Pursuit	SOMP
Support Vector Machines	SVM
Wavelet Packet Transform	WPT

CHAPTER 1. INTRODUCTION

1.1 Brain Computer Interfaces

The human brain is unquestionably the most complex organ of the body as it controls and processes its movement and senses. A healthy brain is able to generate responses to the signals it receives, and transmit messages to the body. Some neural disorders can impair the communication between the brain and the body preventing the transmission of these messages. Brain Computer Interfaces (BCIs) are devices that hold immense potential to assist patients with such disorders by analyzing brain signals, translating and classifying various brain responses, and relaying them to external devices and potentially back to the body. Therefore, such devices may be beneficial for patients suffering from disorders such as spinal cord injury, stroke, amyotrophic lateral sclerosis and a variety of neurological diseases [**1**].

Based on the signal recording modality, the BCI technology can be divided into two major categories: invasive technologies in which neurosurgeons implant arrays of microelectrodes directly into the brain, and non-invasive methods wherein the activity of neuronal populations can be recorded by placing electrodes on the scalp or using imaging techniques such as functional Magnetic resonance Imaging (fMRI).

It is useful to provide some preliminary background about the anatomy and physiology of the brain to better understand brain signals and their relation to the activity of a single neuron.

1.2 Rest potentials

Neurons and glial cells are the main building blocks for the central nervous system (CNS). Generally, a neuron in mammalian CNS consists of a cell body, called *Soma,* that contains the nucleus, *dendrites* and a long fibrous *axon* that originates from an area of the cell body called *axon hillock* [**2**]. Figure 1 illustrates a schematic view of a neuron.

Electrical, chemical or mechanical stimuli can cause excitation in neurons. The responses of the cell to the stimuli can be categorized in two types: electrotonic potentials and action potentials. The former corresponds to non-propagated potentials and the latter refers to propagated potentials.

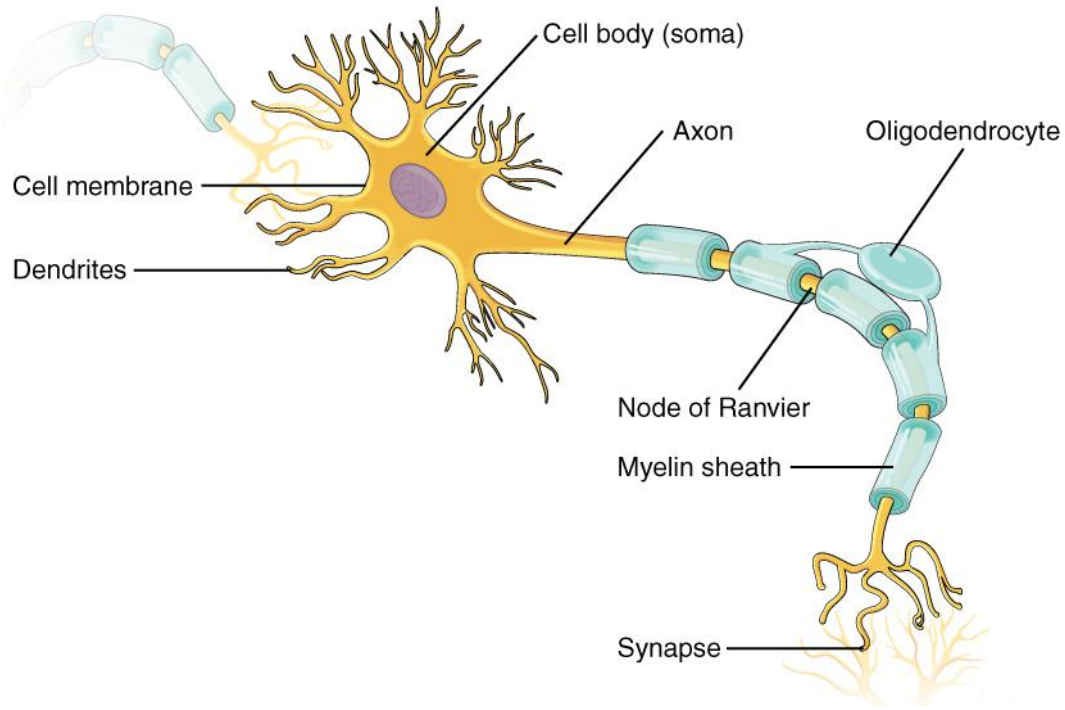

Figure 1 A schematic view of a neuron.
By OpenStax College [CC BY 3.0 (http://creativecommons.org/licenses/by/3.0)], via Wikimedia Commons.

Across the neuron membrane, there exists a variety of ions such as Potassium, Sodium and Calcium ions that have major role in the generation of electrical potentials along the axon. The concentration of these ions across the cell membrane is not uniform. These ions can move across the membrane through channels that are permeable to particular ion types. Because of these two reasons, a potential difference across the membrane, called the rest potential, can be observed. Typical values of the rest potential are equal to -70 mV [**2**]-[**3**]. Figure 2 depicts the rest potential across the cell membrane.

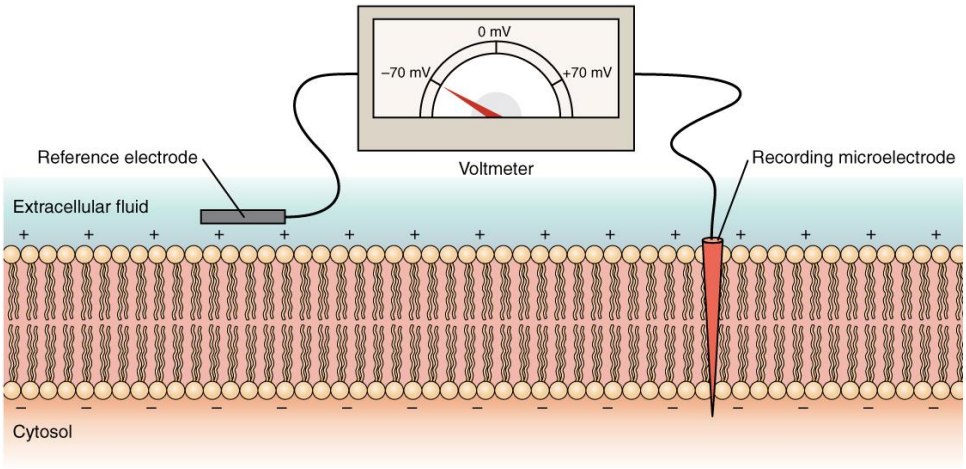

Figure 2 Rest potential across the cell membrane. OpenStax College, The Action Potential. OpenStax CNX. Nov 7, 2014 http://cnx.org/contents/401af334-2930-4731-ba9a-14a346326e63@5.

Potassium ions (K^+) and Sodium ions (Na^+) play an important role in the rest potential. K^+ concentration inside the neurons is much higher than outside, whereas the concentration of Na^+ is higher outside. The concentration gradient of the K^+ ions makes these ions go towards the outside of the cell via the K^+ channels. Similarly the Na^+ ions move towards the inside of the membrane via Na^+ channels. But since the number of open K^+ channels is always greater than Na^+ channels the flow of the K^+ ions toward the outside of the membrane is greater. Meanwhile, the Na^+-K^+ ATPase actively moves the K^+ and Na^+ ions against their electrochemical gradient. Therefore the rest potential remains stable. [**2**]- [**3**].

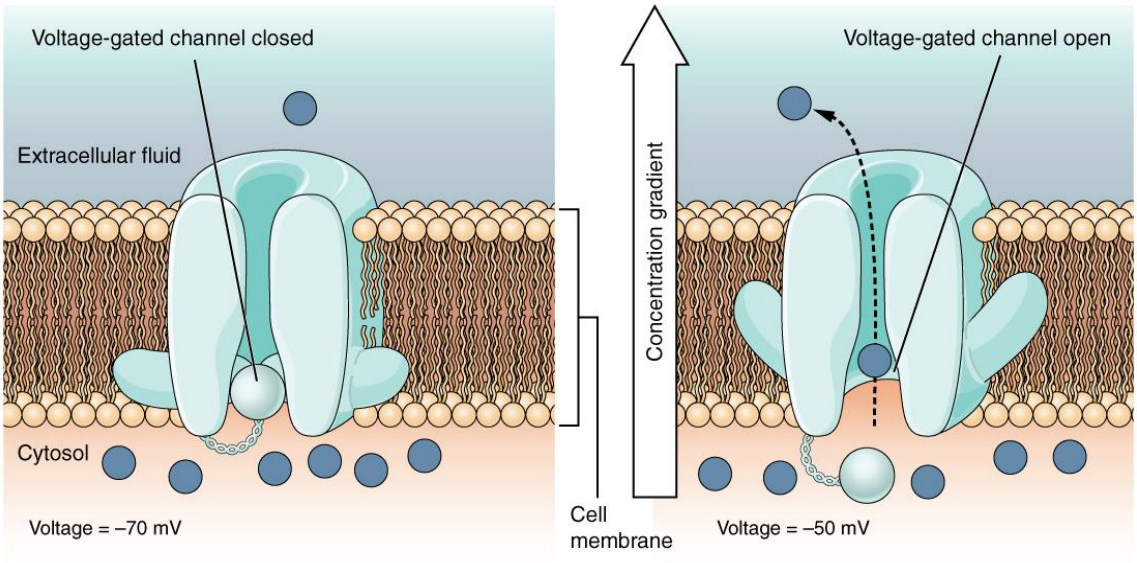

Figure 3 Voltage-Gated Channels. OpenStax College, The Action Potential. OpenStax CNX. Nov 7, 2014 http://cnx.org/contents/401af334-2930-4731-ba9a-14a346326e63@5.

1.3 Action Potentials

There are different types of ion channels in the cell membrane. Some of these channels are gated and sensitive to electrical or chemical stimulation, hence the name voltage-gated and ligand-gated channels. A voltage-gated channel is depicted in Figure 3. When the Na^+ gated channels become active, and when the threshold potential is reached, the Na^+ ions move toward the inside of the membrane, which result in a great increase in the number of Na^+ ions inside the cell and consequently creates a positive potential difference across the membrane that lasts for few milliseconds. This phenomenon is called *depolarization*.

During depolarization, the concentration of Na^+ ions increases inside the membrane and changes the Na^+ gradient toward the outside of the membrane. Meanwhile, K^+ gated channels also get activated, and the K^+ ions move to the outside of the membrane. As a result, the potential difference across the membrane decreases. This phenomenon is called *repolarization*.

The opening procedure of the gated K^+ ion channels is slower than the gated Na^+ ion channels. Therefore the permeability to K^+ ions increases following the increase in Na^+ permeability. Moreover, the slow closing procedure of the gated K^+ channels makes more K^+ ions leave the membrane. This phenomenon is called *hyperpolarization* [**2**]-[**3**]. An action potential is illustrated in Figure 4.

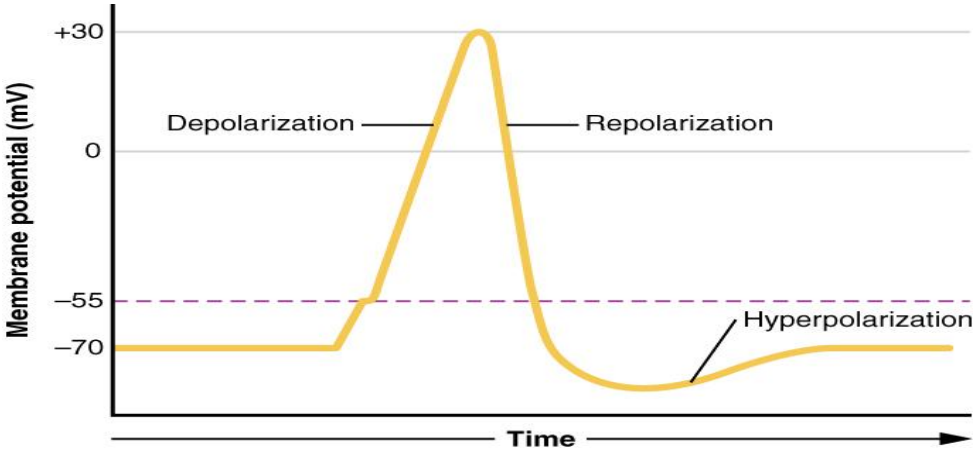

Figure 4 Action potential. OpenStax College, The Action Potential. OpenStax CNX. Nov 7, 2014 http://cnx.org/contents/401af334-2930-4731-ba9a-14a346326e63@5.

So far, we have discussed the response of a single neuron. In the next section Electroencephalograms (EEGs) and their relation with a single neuron activity are introduced.

1.4 Electroencephalography

The background electrical activity of the brain in unanesthetized animals was first described qualitatively in the 19th century, but the German psychiatrist Hans Berger was the first to analyze the variations in the brain potential in a systematic way and introduced the term electroencephalogram (EEG) in 1924 [**4**]. EEG signals recorded from the scalp represent an important electrical activity on the cortex and dendrites of the pyramidal cortical cells. In fact, the EEG mostly measures an aggregate effect of dendritic postsynaptic potentials since the superficial layers of the cerebral cortex are covered by the dendrites as shown in Figure 5 [**2**]-[**4**].

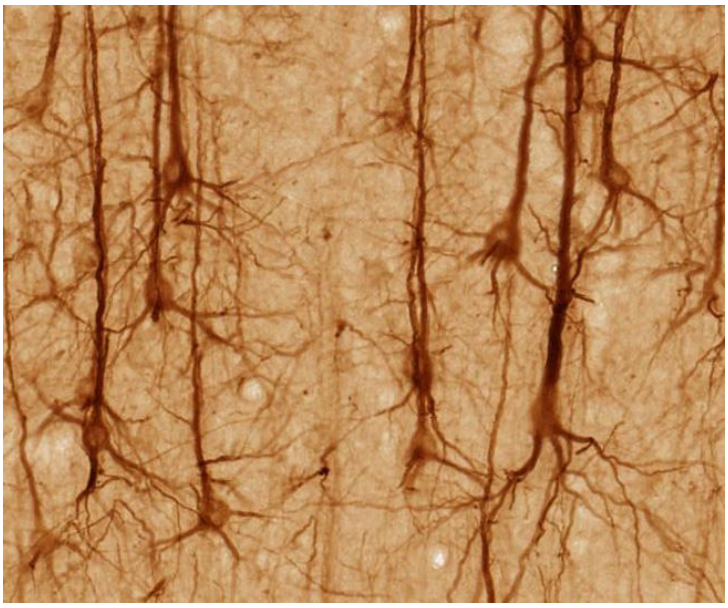

Figure 5 The pyramidal cells of cerebral cortex. By UC Regents Davis campus (http://brainmaps.org) [CC BY 3.0 (http://creativecommons.org/licenses/by/3.0)], via Wikimedia Commons.

The Brain electrical activity is usually recorded using three modalities [**4**].

1. Scalp electrodes that allow a non-invasive recording of the brain electrical activity.
2. Cortical electrodes that are placed on the cortex of the brain. This method can be considered as an invasive approach. This recording is called Electrocorticography (ECoG).
3. Depth recording, which is an invasive method that requires inserting needle electrodes into the brain.

The recorded electrical potentials of the brain is a superposition of the electrical activity of all neuronal populations, but being close to the source of the activity can generate better spatial

resolution and also higher Signal to Noise Ratio (SNR). Owing to the non-invasive process whereby these signals are recorded, EEG is an attractive modality for BCI and is the main focus of this thesis. The international federation 10-20 system is typically used to record the EEG signals (Figure 6). This system was introduced to standardize the placement of the electrodes for all the subjects. Bipolar Montage refers to measuring the difference between two adjacent electrodes and referential montage describes the measurement with respect to a reference electrode.

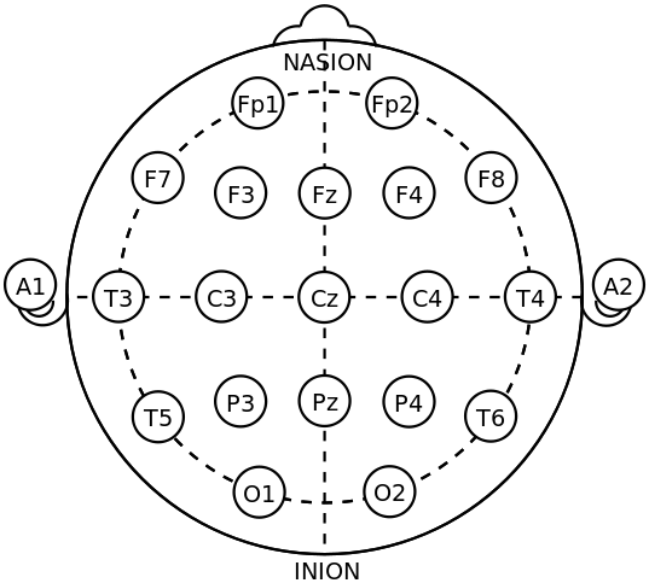

Figure 6 The international 10-20 system to place the electrodes on the scalp.

1.5 Anatomic study of the brain

The CNS consists of the spinal cord and the brain. The brain is divided into three main parts: Brainstem, Cerebellum and Cerebrum. The brainstem is a short extension of the spinal cord and is a connection between the cerebral cortex, the spinal cord and the cerebellum. It is also an integration center for motor refluxes. The cerebellum maintains the balance of the body muscle movement, while the cerebrum is responsible for conscious functions [**2**]-[**3**].

Within the CNS, there are ascending nerve tracts originating from the spinal cord that deliver information to the brainstem (such as pain or touch) and descending nerve tracts that connect brain divisions such as cerebrum and cerebellum to the motor neurons and therefore control the activity of the skeletal muscles.

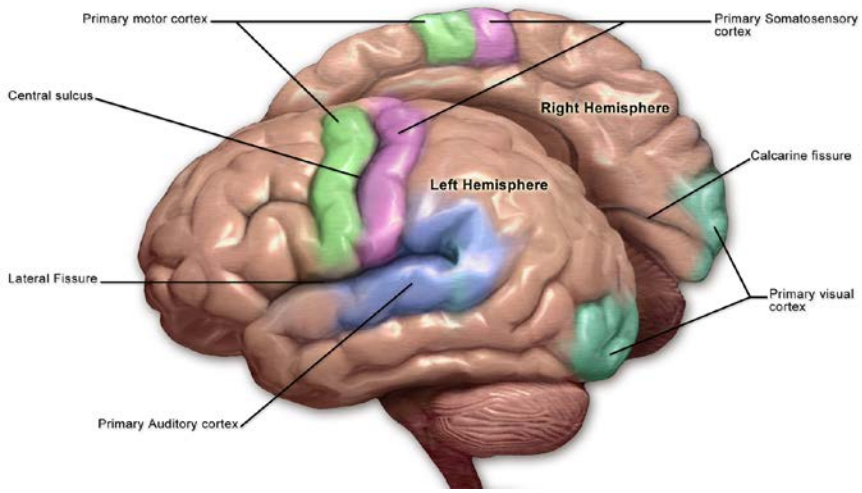

Figure 7 The primary motor cortex By BruceBlaus, Blausen.com staff. "Blausen gallery 2014". Wikiversity Journal of Medicine. DOI:10.15347/wjm/2014.010. ISSN 20018762. (Own work) [CC BY 3.0 (http://creativecommons.org/licenses/by/3.0)], via Wikimedia Commons.

Motor imagery EEG signals, the primary focus of this thesis, are recorded when the subjects are asked to imagine the movement of a particular limb. Hence, preliminary background on how movement is planned in the brain is presented. The brain must plan the movement and maintain all the necessary motions at the same time before moving a limb. The cortex, the basal ganglia and the lateral portion of the cerebellar hemisphere are generally involved in planning the movement; therefore the electrical activity in this region highly increases before the movement. The motor cortex and premotor cortex receive the information via the thalamus, and then relay this information to the spinal cord via corticospinal tracts and corticobulbar tracts to motor neurons in the brain stem **[2]**.

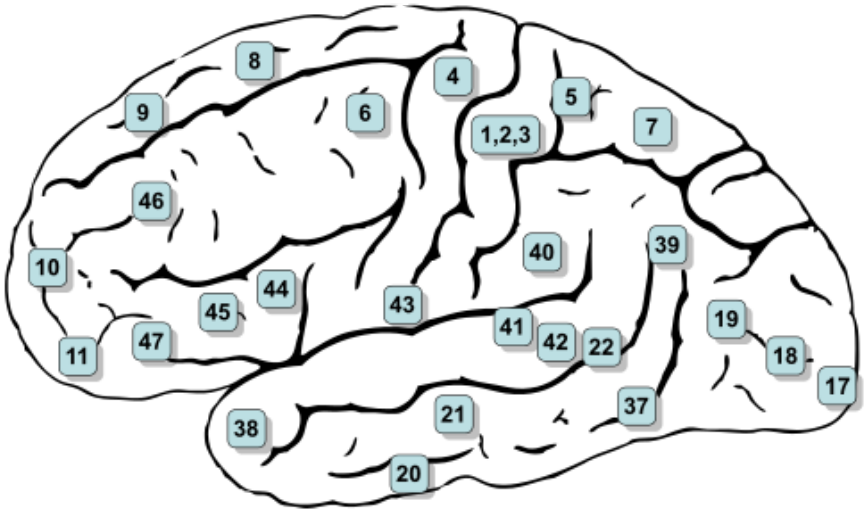

Figure 8 Bordmann's area numbers.

It has been realized through stimulation experiments in craniotomy under local anesthesia, and also imaging techniques such as fMRI, that the primary motor cortex (Brodmann's area 4 or M1 Figure 8) is involved in voluntary movement. The primary motor cortex is located in the percentral gyrus as shown in Figure 7, and most of the body movement and postures are projected on this area such as face on the bottom and feet movement on the top of the gyrus. Figure 9 illustrates disproportionate map of the body in the motor cortex. While the premotor cortex (Bordmann's area 6) functionality is still not fully understood, it is believed that it is mostly involved in setting postures at the beginning of a planned movement **[2]**.

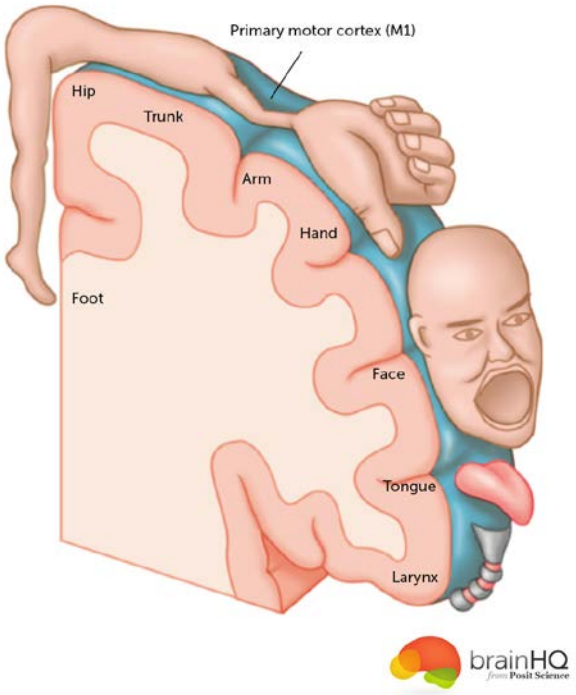

Figure 9 A figurative representation of the body map in the primary motor cortex.

1.6 Thesis outline

The primary objective of this work is to develop classification algorithms that are computationally efficient and that use a small number of measurements to support real-time BCI. In this thesis, we explore a range of techniques to extract useful features and to classify motor imagery EEG signals based on sparse representations [**5**] and multiresolution analysis.

Event-Related Synchronization/Desynchronization (ERS/ERD) are known as important phenomena that occur during movement, pre-movement and movement imagination. Therefore a preliminary background about the concepts of ERD/ERS is necessary and is described in chapter 2.

In the proposed approach, features from neighboring electrodes in a small spatial region are approximated by a sparse linear combination of a few atoms from a dictionary constructed from training sets corresponding to the different classes. The class of each EEG trial is then determined from the sparsity pattern of the recovered vector.

Since electrodes in a small spatial neighborhood are recording activities related to neighboring neural populations, it is conceivable that leveraging the correlation between these recordings could enhance the classification performance. To this end, we propose a joint sparsity model that exploits correlation between neighboring electrodes [**6**]. Sparse representation of the signals and joint sparsity are presented in chapter 3.

In this thesis, a variety of feature vectors based on wavelet characteristics of the EEG trials are extracted, including Wavelet coefficients, energy of the signals in different frequency sub-bands, entropy of the signals, and also a combination of energy and entropy. Power-related features have been employed in the classification of motor imagery EEG signals in related work [**7**]. In contrast to [**7**], which is based on the energies of spatial projections, in this work we use energies

in different frequency sub-bands motivated by the existence of different levels within the alpha band of interest. While [**8**] uses average power in various sub-bands, their classification approach is based on support vector machines unlike the sparsity approach proposed herein.

Also, we use entropy as an additional feature for classification. Entropy as a single entry feature is able to capture the distribution of the trials and it was shown to be effective for classifying EEG recordings from normal subjects and epileptic patients [**9**]. Therefore, in the final approach the entropy is also concatenated to the energy vectors to enhance the feature vectors.

The methodologies and simulation results are described in detail in chapter 3. Chapter 4 contains the summary and conclusion of this thesis as well as future directions.

CHAPTER 2. EVENT-RELATED DESYNCHRONIZATION

2.1 Introduction

Using EEG signals as a non-invasive method to record and study the behavior of the brain is prevalent. Nevertheless, EEGs are highly sensitive to noise. This calls for advanced signal processing methods to extract meaningful features that are pertinent to different physiological phenomena. Moreover, knowledge of EEG signals and their characteristics (such as bandwidth and amplitude), can be very beneficial for extracting more useful and representative feature vectors. In this chapter, Event-Related Potentials (ERP) and Event-Related Desynchronization (ERD) are introduced. These are known oscillations in EEG signals that are associated with different events.

Hans Berger discovered that the brain generates rhythmic potentials [**10**] and these oscillatory activities are believed to be the result of synchronous neuronal populations in different cortex areas. Generally speaking, the frequencies of these oscillations could depend on the membrane properties of different neurons, as well as how they are organized and connected in the underlying networks [**11**].

EEG signals can be classified into five categories, based on their frequency bands:

1. *Delta Waves:* These are low frequency signals below 3.5 Hz and mostly occur when a person is asleep.

2. *Theta Waves:* These consist of signals in the frequency range 4-7 Hz. They can be observed in the Parietal and Temporal lobes in babies, as well as adults who are suffering from anxiety. Figure 10 shows the brain lobes.

3. *Alpha Waves:* These are rhythmic waves in the frequency band 8-13 Hz and can be observed in normal people in a relaxed and conscious state. This class of waves occurs in the Occipital lobe with higher amplitude, but they can also be recorded in the Frontal and Parietal lobes.

4. *Beta Waves:* These consist of signals in the frequency range 14-30 Hz and can be recorded in the Parietal and Frontal lobes. They are mostly present when a person has some high neural activity and tensions. When a conscious person concentrates on a subject, the Beta waves that are unsynchronized waves with lower amplitudes, will replace the Alpha waves.

5. *Gamma Waves:* The frequency of this class is higher than 35 Hz.

An important neural activity termed rolandic mu rhythm was later discovered (See [**12**] and references therein). This neural activity carries physiological information and is part of the alpha band recorded over the sensorimotor cortex.

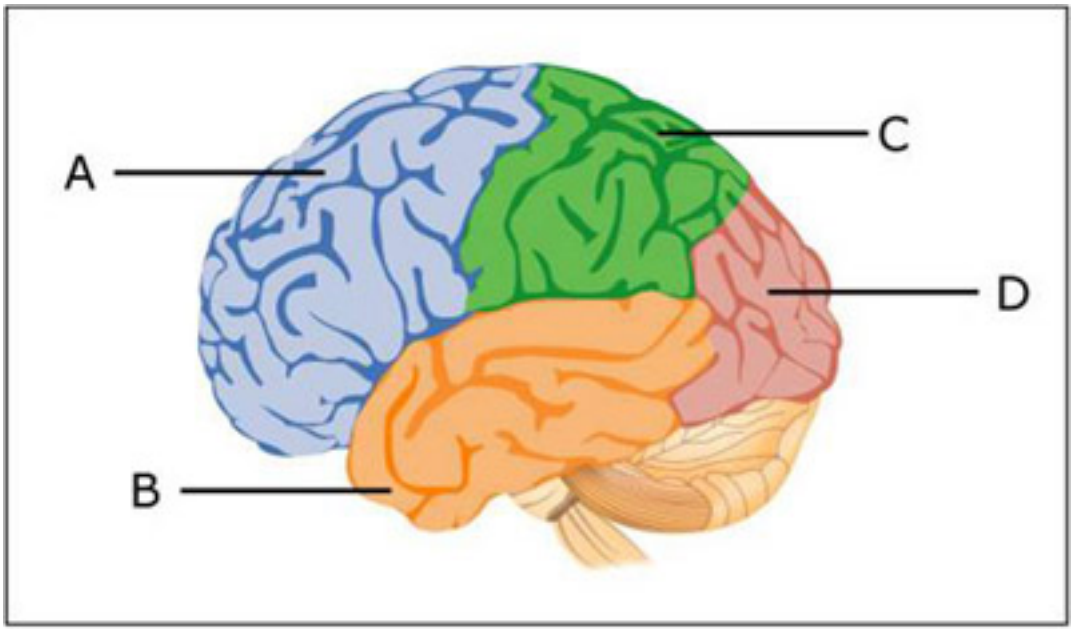

Figure 10 Lobes of the brain. A. Frontal lobe, B. Temporal lobe, C. Parietal lobe and D. Occipital lobe (Image by MIT OpenCourseWare.)

Brain activity is related to different events and types of stimuli. For example, a sensory stimulus can cause changes in the activity of neuronal populations. Such changes are called Event-Related Potentials (ERPs) [**13**]. Evoked Potentials such as Visual Evoked Potentials (VEP) and Auditory Evoked Potentials (AEP) are good examples of such changes. ERPs are phase-locked activities, i.e., evoked oscillations with a fixed time delay from the stimuli. Therefore, averaging techniques can enhance the signal to noise ratio and help to observe the ERPs [**13**].

2.2 Event-Related Desynchronization

Certain events can induce a response such as blocking or desynchronizing the ongoing alpha activity, which may be observed in the EEG. The work in [**13**] provides an excellent review of two types of event-driven changes in the power of the EEG signals in particular frequency bands called Event-Related Desynchronization/Synchronization (ERD/ERS).

1. Event-Related Desynchronization (ERD) that is based on decrease in power in given frequency bands.
2. Event-Related Synchronization (ERS) that is based on an increase in power in given frequency bands.

Pfurtscheller and Aranibar introduced the concept of ERD in 1977. Numerous studies have focused on developing and deriving features based on ERDs related to different events. Generally, ERD and ERS are non-phase locked or induced responses [**14**]. Pfurtscheller provided four processing steps for ERD and ERS: (i) Band pass filtering, (ii) squaring the amplitudes to obtain the instantaneous power of the samples in time, (iii) averaging over trials and (iv) time averaging for smoothing purposes [**13**].

As mentioned above, ERD is the desynchronization or decrease in EEG's power in a specific frequency band that identifies activation of neuronal population in specific locations. On the other hand, ERS represents deactivation or inhibition in neuronal population. These phenomena are related

to the Cortical Activation (CA). According to [**15**], when there are considerable cortical activities in neuronal populations, there is a smaller number of non-occupied neurons, therefore an increase in CA can induce ERD. After the movement or motor imagery, when cortical activity is inhibited, there are more free neurons available and ERS can occur [**15**].

In essence, during motor execution and even motor imagery ERD represents a synchronous activity of the cortical area, and ERS represents deactivated or inhibited cortical networks [**11**]. While ERD/ERS are frequency band specific, ERPs are not, which is the main difference between ERP and ERD/ERS [**13**].

The ERD related to mu rhythm is most prominent over sensorimotor areas during motor preparation [**12**]. Two types of rolandic mu rhythm can be distinguished in the alpha band, the lower-frequency mu rhythm between 8-10 Hz and the higher frequency mu rhythm between 10-13 Hz. While the lower frequency rhythm shows an ERD pattern that is indistinguishable for finger or foot movement, an ERD pattern that is movement-type specific (distinct for finger and foot movement) can be observed in the higher frequency mu rhythm [**11**].

It is well known that Desynchronizing the mu rhythm or enhancing the mu rhythm is a result of the movement-related events, and also imagination of limbs movement. Therefore, they can be considered as appropriate features to develop an EEG-based BCI with motor imagery. For instance, it was shown by Pfurtscheller and Neuper that foot and tongue movement, and also foot movement

imagination, can enhance the mu rhythm, but hand movements or finger movements and imagination of hand movements can desynchronize the mu rhythm [**16**]-[**17**].

Referring to ERD/ERS changes should be associated with frequency band specification. [**13**]-[**18**] have defined ERD as

$$ERD(t) = \frac{Power(t) - Reference\ Power}{Reference\ Power} \quad (1)$$

Here Reference power is defined as the pre-stimulus power of the signal and $power(t)$ denotes the instantaneous power.

The features corresponding to ERD/ERS were defined in [**19**] as

$$f^{ERD} = mean(|x^{ERD}|) \quad (2)$$

where x is the preprocessed EEG signal.

We applied equation (2) on motor imagery EEG signals related to hand and tongue movements (Figure 11). In hand movement imagination illustrated in blue, we can see de-synchronization of the EEG whereas in tongue movement imagination we observe an increase in power.

Since feature vectors based on power and power changes such as ERD and ERS are helpful to make different motor imagery classes separable, in this work mostly power-related features are employed to perform the classification on the available datasets.

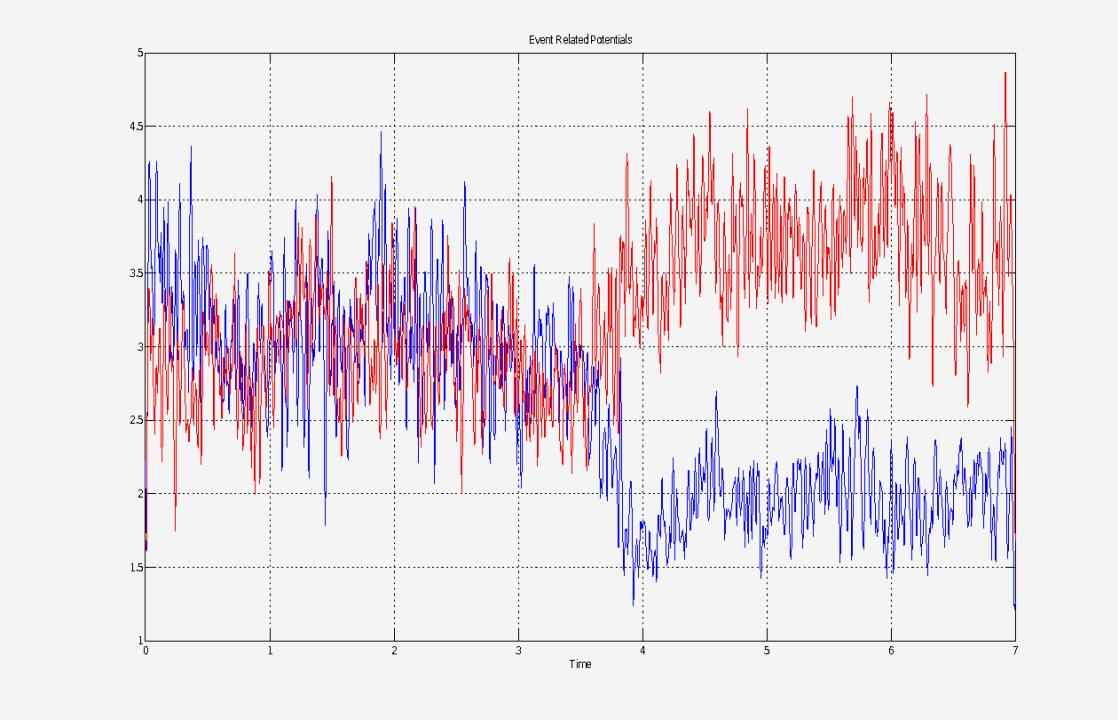

Figure 11 ERD related to the class 1 and four of the dataset 3a. ERD related to hand movement is shown in blue and ERS related to tongue movement is shown in red color.

CHAPTER 3. CLASSIFICATION OF EEG SIGNALS USING SPARSE REPRESENTATIONS

In this chapter, we begin with a brief review of sparse representation of signals, since it is the main part of the classification techniques in this thesis. Signal processing techniques relevant to EEGs, our proposed methods, and simulation results are provided in this chapter.

3.1 Introduction to sparsity

Sparse signal representations have received significant attention in recent years [**20**]- [**21**]- [**6**]. A vector is said to be sparse when most of its entries are zero or close to zero and only a few of them are nonzero. Consider an $n \times 1$ column vector s, with K nonzero values. When $K \ll n$ vector s is called K-sparse. It is possible to compress this signal as follows

$x = \mathrm{A}s$

$$\begin{bmatrix} x_1 \\ x_2 \\ \vdots \\ x_B \end{bmatrix} = \begin{bmatrix} a_{11} & a_{12} & \dots & a_{1n} \\ a_{21} & a_{22} & \dots & a_{2n} \\ \vdots & \vdots & \vdots & \vdots \\ a_{B1} & a_{B2} & \dots & a_{Bn} \end{bmatrix} \begin{bmatrix} s_1 \\ s_2 \\ . \\ . \\ . \\ s_n \end{bmatrix} \quad (3)$$

where A is called the measurement matrix. Finding the vector s from the measurements x is generally not possible since (3) is an undetermined system of linear equations. However, if s is known to be sparse, it may be uniquely recovered from x [**22**]. Many sufficient conditions were

established to ensure perfect recovery of sparse vectors such as the celebrated Restricted Isometry Property (RIP) **[20]**, **[21]**.

A matrix A obeys the RIP property of order K if:

$$(1-\delta_k)\|s\|_{\ell 2}^2 \leq \|As\|_{\ell 2}^2 \leq (1+\delta_k)\|s\|_{\ell 2}^2 \quad (4)$$

is satisfied for all K-sparse vectors s. δ_K is the isometric constant of a matrix A. In a nutshell, RIP implies that all subsets of K columns taken from matrix A are nearly orthogonal [**5**].

3.2 Single sparse representation of EEG signals

In this work, we approximate the measurement vectors by linear combinations of a small number of atoms from a dictionary. The EEG feature vector $x \epsilon \mathbb{R}^{\boldsymbol{B}}$ belonging to class m, is written as a linear combination of N_m training samples in the dictionary from class m. Hence,

$$x = \begin{bmatrix} x_1 \\ x_2 \\ \vdots \\ x_B \end{bmatrix} \approx \begin{bmatrix} a_{11}^m & a_{21}^m & \dots & a_{N_m 1}^m \\ a_{12}^m & a_{22}^m & \dots & a_{N_m 2}^m \\ \vdots & \vdots & \vdots & \vdots \\ a_{1B}^m & a_{2B}^m & \dots & a_{N_m B}^m \end{bmatrix} \begin{bmatrix} \alpha_1^m \\ \alpha_2^m \\ . \\ . \\ . \\ \alpha_{N_m}^m \end{bmatrix} = A^m \alpha^m \quad (5)$$

where A^m is a $B \times N_m$ matrix called the class m subdictionary, and α^m is the sparse representation of x that has only K non-zero values.

The training set belonging to class m is used to generate the columns of the m-th subdictionary. Training samples from M classes generate M subdictionaries of a $B \times N$ dictionary A, where $N = \sum_{m=1}^{M} N_m$. We can readily write the sparsity model as,

$$x \approx [A^1 \quad A^2 \quad \dots \quad A^m] \begin{bmatrix} \alpha^1 \\ \alpha^2 \\ \cdot \\ \cdot \\ \cdot \\ \alpha^M \end{bmatrix} = A\alpha \qquad (6)$$

If the test trial belongs to class m, we anticipate the representation to be mostly supported on the m-th subdictionary, i.e., that most of the non-zero values of the sparse vector α would correspond to columns of the m-th subdictionary.

Therefore, the test signal is approximated using K atoms from the dictionary as

$$x = \alpha_{\lambda_1} a_{\lambda_1} + \alpha_{\lambda_2} a_{\lambda_2} + \cdots + \alpha_{\lambda_k} a_{\lambda_k} \qquad (7)$$

where $\Lambda = \{\lambda_1, \lambda_2, \dots, \lambda_k\}, k = 1, \dots, K$ is the support of the sparse vector. To recover the sparse vector α, we need to solve the following optimization problem

$$min\|\alpha\|_0$$

$$subject\ to\ A\alpha = x \quad (8)$$

This problem is generally NP-hard. It can be written as

$$min\|A\alpha - x\|_2$$

$$subject\ to\ \|\alpha\|_0 \leq K_0 \quad (9)$$

where K_0 is an upper bound on the sparsity level. In this work, the well-known Orthogonal Matching Pursuit (OMP) greedy algorithm [**23**] is used to solve this problem.

After obtaining the sparse representation $\hat{\alpha}$ of a test signal, it can be classified by computing M residuals as

$$r^m(x) = \left\|x - A^i\hat{a}^m\right\|_2, m = 1,2, \dots, M \quad (10)$$

where $\hat{a}^m$ denotes the entries of the sparse vector associated with the m-th-class subdictionary. We choose the class that provides the minimum residual, i.e.

$$class(x) = arg_{m=1,2,\dots,M} min\, r^m(x) \quad (11)$$

3.3 Joint sparse representation of EEG trials

Neighboring electrodes close to the sensorimotor cortex record the oscillations related to pre-movement, movement, as well as movement imaginations. Based on the movement, these electrodes record the event-related changes. Assuming spatial correlation across neighboring electrodes, it is possible to define a joint sparsity model. To this end, instead of considering one feature vector at a time, we use a collection of feature vectors simultaneously to find the joint sparse representation of these vectors. While the atoms are common, the response of each electrode is formed using different values for the set of coefficients. To clarify, assume x_c is a response from a center electrode and we have a $B \times N$ structured dictionary A. The sparse representation of x_c can be written as:

$$x_c = A\alpha_c = \alpha_{c,\lambda_1} a_{\lambda_1} + \alpha_{c,\lambda_2} a_{\lambda_2} + \cdots + \alpha_{c,\lambda_k} a_{\lambda_k} \quad (12)$$

where $\Lambda_k = \{\lambda_1, \lambda_2, \dots, \lambda_k\}$ is the support of the sparse vector. Since neighboring electrodes record similar oscillation patterns with respect to the cue, the response x_j of a neighboring electrode can also be approximated using the same atoms from training set samples within the dictionary, but with different weights. Therefore, all the neighboring electrodes share a common support, but the responses from different electrodes assume different values on the support. Thus,

$$x_j = A\alpha_j = \alpha_{j,\lambda_1} a_{\lambda_1} + \alpha_{j,\lambda_2} a_{\lambda_2} + \cdots + \alpha_{j,\lambda_k} a_{\lambda_k} \quad (13)$$

Consider T electrodes in a small neighborhood around the center electrode x_c, and a structured dictionary A. The responses can be represented by,

$$X = [x_1 \quad x_2 \quad \dots \quad x_T] = [A\alpha_1 \quad A\alpha_2 \quad \dots \quad A\alpha_T] = A\,[\alpha_1 \quad \alpha_2 \quad \dots \quad \alpha_T] = AS \quad (14)$$

where $X = [x_1 \quad x_2 \quad \dots \quad x_T]$ is a $B \times T$ matrix, and x_j is the feature vector of the EEG recorded by electrode j. The matrix S is a row sparse matrix since $[\alpha_1 \quad \alpha_2 \quad \dots \quad \alpha_T]$ share the same support. The jointly sparse matrix S can be recovered by solving the following problem

$$min\|S\|_{row,0}$$
$$subject\ to\ AS = X \quad (15)$$

$\|S\|_{row,0}$ is the number of non-zero rows of S. Since the dictionary $A \in \mathbb{R}^{B \times N}$, the recovered jointly sparse matrix $\hat{S}$ is an $N \times T$ matrix. The problem can be rewritten as

$$\hat{S} = arg\ min\|AS - X\|_F$$
$$subject\ to\ \|S\|_{row,0} \leq K_0 \quad (16)$$

where $\|.\|_F$ denotes the Frobenius norm. This problem can be solved approximately using greedy algorithms. In this work, we used a generalized OMP algorithm called simultaneous OMP (SOMP) [**24**]. The SOMP algorithm is quite similar to the OMP algorithm for the most part. The support is updated iteratively by solving,

$$\lambda_k = argmax_{i=1,2,\dots N} \|R_{k-1}^T \alpha_i\|_2 \quad (17)$$

where R_{k-1} is a residual matrix at the k-th iteration. A summary of The SOMP algorithm is as follows:

Input: $B \times N$ dictionary and the measurement vectors from neighboring electrodes.

$$X = [x_1 \quad x_2 \quad \dots \quad x_T] \quad (18)$$

At the first step, the residual is initialized as $R_0 = X$, and support set as $\Lambda_0 = \emptyset$. In each iteration the index of the atom in the dictionary that provides the best approximation for the measurement matrix is found as,

$$\lambda_k = argmax_{i=1,2,\dots N} \|R_{k-1}^T \alpha_i\|_p \, , p \geq 1 \quad (19)$$

The index set is updated such that $\Lambda_k = \Lambda_{k-1} \cup \{\lambda_k\}$ where Λ_k denotes the support set at the k-th iteration. Then a least-square problem is solved to obtain a new signal estimate or we simply compute

$$\mathrm{P}_k = \left(A_{\Lambda_k}^T A_{\Lambda_k}\right)^{-1} A_{\Lambda_k}^T X \quad (20)$$

where A_{Λ_k} consists of k columns in A indexed in Λ_k. The new residual is calculated

$$R_k = X - A_{\Lambda_k} P_k \quad (21)$$

The iterations continue until a stopping criteria is met. At termination, the index set Λ identifies the nonzero rows of the sparse matrix $\hat{S}$ and the values are the K rows of the matrix P_k.

To complete the classification, the error residual between the original test samples and the approximation obtained from sub-dictionaries can be calculated as,

$$r^m(X) = \left\| X - A^m \hat{S}^m \right\|_F, m = 1,2, \dots, M \quad (22)$$

where $\hat{S}_m$ are the rows associated with the sub-dictionary of the m-th class. If atoms of a sub-dictionary have greater weights in the recovered sparse matrix, the error residual for that

particular mth-class sub-dictionary would be smaller, therefore the label of the classes are chosen to minimize the residual, i.e.,

$$class(x_c) = argmin(\, r^{m}_{n=1,2,\dots,M}\,(X)) \qquad (23)$$

3.4 Introduction to EEG processing

Biomedical signals, especially EEGs are vulnerable to noise which calls for advanced signal processing methods to process these signals for applications such as monitoring, diagnostic devices and brain computer interfaces. Various noise sources can degrade the quality of EEG recordings, including external sources (outside of body), as well as some natural biomedical signals. For instance, biomedical signals close to the EEG electrodes such as Electromyograms (EMG) can interfere with EEG signals. Also, blinking and eye movement called electro-oculogram (EOG) is a major source of noise for EEGs. Motion artifacts are also an important issue that has to be handled properly during the procedure of recording the signals of subjects. The quality and the material of the electrodes, the liquid that is used as the electrolyte on the skin, and even 50/60 Hz electrical noise induced by electricity lines are examples of external noise sources that can augment the EEGs processing difficulties [**4**].

Biomedical signal processing can be generally divided into three major steps: 1-Pre-Processing 2-Feature extraction 3-Classification.

A general block-diagram of a Biomedical Signal Processing unit is shown in Figure 12.

Figure 12 A block diagram of a BSP unit.

Pre-processing is a major step in biomedical signal processing to enhance the SNR before the feature extraction and classification steps. For instance, it is usually recommended to employ Band Pass Filters (BPF) to remove the effects of EMGs, and also a notch filter on 50/60 Hertz to remove the 50/60 induced electrical noise. Two electrodes are usually placed near the eyes to record the EOGs to cancel their effect. Other electrodes on the scalp record the main EEG signals in addition to the unwanted EOG signals. Therefore, it is possible to remove the eye movement effect, by subtracting them from the signals recorded on the scalp. To solve the motion artifacts problem, silver/silver-chloride (Ag/AgCl) electrodes are widely used nowadays since they are more robust to motion [**4**].

EEG signals are very complex signals and different signal processing methods have been used individually or simultaneously to extract the best features possible for the appropriate application. Methods like Wavelet Transforms [**8**], and autoregressive coefficients [**25**] are some of the notable methodologies. Furthermore, choosing a classification technique best suited for the

feature vectors can improve the results in terms of accuracy and computational complexity. Linear Discriminant Analysis (LDA) [**25**] and Support Vector Machines (SVM) [**26**], are some of the most widely used classification methods.

3.5 Dataset

Two sets of data provided by BCI competitions, are used in this work.

1. *Dataset 3a:* This is a multi-class, cued motor imagery EEG data with 4 classes (left hand, right hand, foot, and tongue). A 64-channel EEG amplifier from Neuroscan is used to record the signals. The left mastoid is used as reference and the right mastoid is considered as ground. The recorded signals are filtered between 1 and 50 Hz, and a notch-filter is used.

Subjects performed motor imagery for left hand, right hand, foot and tongue movement according to a cue. Each subject completed the experiment for at least 6 runs; each run consists of 40 trials for each class. For instance, one of the subjects performed 9 runs; therefore there are 90 trials for each class and 360 trials in total.

To record the signals, the subjects sat in a relaxing chair with armrests. At the beginning of the trials, the first 2 seconds were quiet. At t=2, the beginning of the trial was announced using an acoustic stimulus and a cross "+" on the screen, but still the cue to indicate the task was not shown. At t=3 seconds, an arrow to the left, right, up or down was displayed for 1 second to indicate the motor

imagery task, and at this time the subjects were asked to *imagine* the indicated task (i.e. left hand, right hand, foot or tongue movement), until the cross disappeared at t=7 seconds. 60 channels were used in this experiment and the recorded EEG was down-sampled to 250 Hz. Figure 13 shows the position of the channels. In this thesis, only signals related to one of the subjects is used.

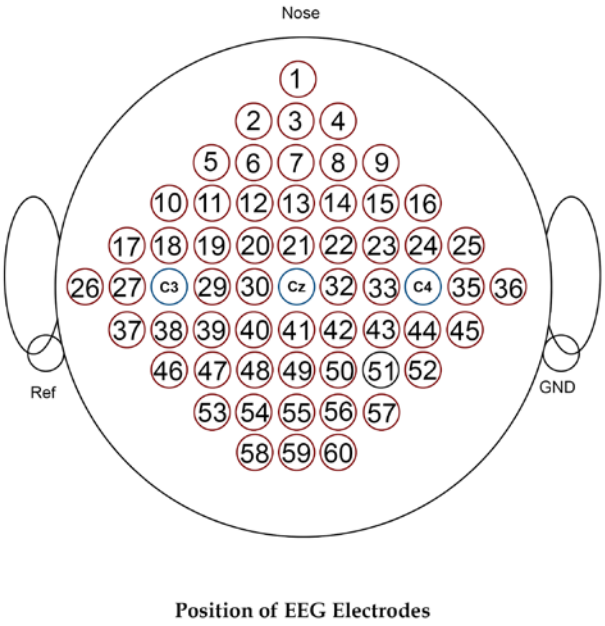

Figure 13 Channel locations in database3a.

2. The Second database is *dataset 4a* provided by Fraunhofer FIRST, Intelligent Data Analysis Group (Klaus-Robert Muller, Benjamin Blankertz), and Campus Benjamin Franklin of the Charite-University Medicine Berlin, Department of Neurology, Neurophysics Group (Gabriel Curio).

This data set consists of signals of five healthy subjects. Visual cues indicate the motor imagery task that each subject should perform, i.e., L for Left hand, R for right hand and F for foot movement. The visual indicator lasts for 3.5 seconds for every trial then a rest period begins with a random length of 1.75 to 2.25 seconds. Two different types of visual stimulation were used: 1) Cues are letters behind a fixation cross; 2) A randomly moving object indicated targets.

Signals were recorded while subjects sat in a comfortable chair with armrests. The signals were recorded using BrainAmp amplifiers and a 128-channel Ag/AgCl electrode cap from ECL. 118 EEG channels were measured at the positions of the extended international 10/20 system. Signals were band-pass filtered between 0.05 and 200 Hz and digitized at 1000 Hz with 16-bit accuracy. For each subject there are 280 trials with 118 EEG channels and the time positions of the 280 cues are also provided for all of the subjects. It is important to note that, they have only provided the cues for classes “right hand” and “foot”, so there are 140 trials for class 1 and 140 trials for class 2. Figure 14 illustrates the location of the electrodes for dataset4a.

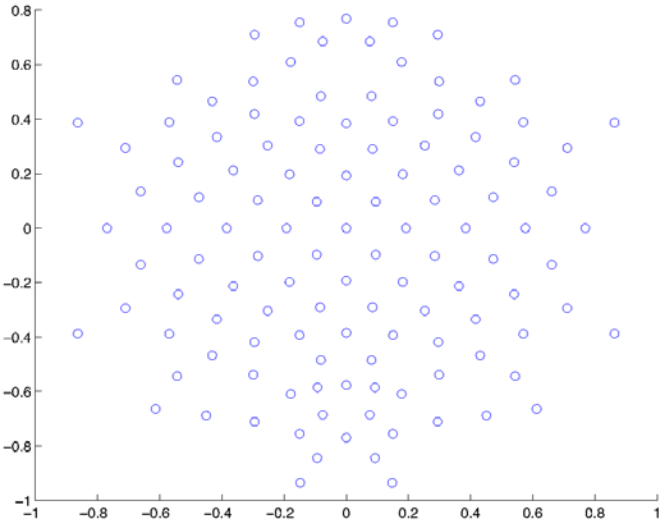

Figure 14 Location of electrodes for dataset 4a.

3.6 Pre-Processing

To enhance the SNR, using band-pass filters is inevitable. Chapter 2 underscored the importance of mu rhythms and their specifications in motor imagery EEGs. It is known that the brain responses to the movement and pre-movement planning mostly occur in mu rhythms. Therefore, a Butterworth band pass filter of order 700 with pass band between 8-12 Hz is used to preprocess the raw signals. The frequency response of the BPF is depicted in Figure 15.

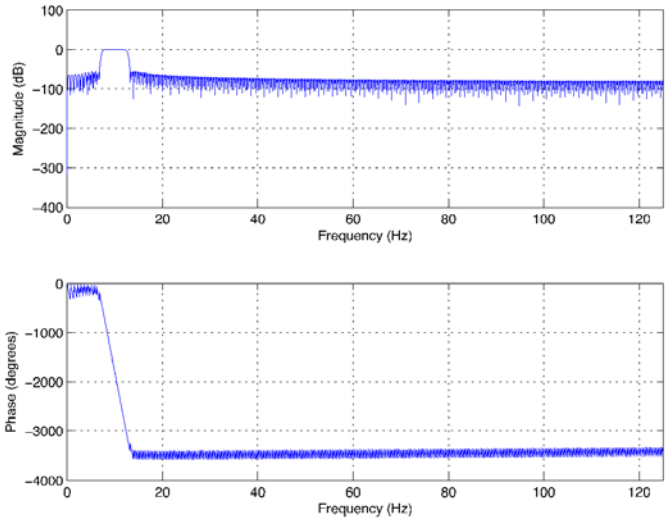

Figure 15 BPF Frequency Response used in the pre-processing step.

Using projection techniques such as Principle Component Analysis (PCA) can potentially reduce the dimensions of the data and may lead to better discriminant features. One of the most promising techniques in EEG signal processing is Common Spatial Patterns (CSP) [**18**]- [**29**]. This method has been introduced by Z. J. Koles [**30**] and then applied to the classification of movement related EEG by Muller-Gerking, et. Al [**31**]. Ramoser developed the technique to classify the hand motor imagery trials [**29**].

CSP aims to project the data along a direction for which the trials from one class have maximum variance and the trials from the other class have minimum variance. We used this technique as a preprocessing step to project the trials from different classes, thereby reducing the

dimensionality of the data while maintaining the separation between the classes. To accomplish this goal, the method uses simultaneous diagonalization of two covariance matrices.

In CSP, two normalized spatial covariance matrices of the EEG trials are calculated, one for each class. Let Y denote the $N \times Q$ matrix of pre-processed single trial EEG data, where N is the number of the channels and Q is the number of samples per channel. The normalized spatial covariance matrix of the EEG trial can be calculated as

$$C_i = \frac{YY^T}{Trace(YY^T)} \quad (24)$$

Here Y is the single trial signal, $Trace(A)$ is the summation of diagonal entries of a matrix A ,and ^{T} denotes transposition. Then, the composite spatial covariance can be formed as

$$C_c = \bar{C}_1 + \bar{C}_2 \quad (25)$$

$\bar{C}_1$ and $\bar{C}_2$ denote the average of the covariance matrices of all the trials in classes 1 and 2, respectively. The dimension of the obtained covariance matrices is $N \times N$. The covariance matrices are transformed to S_1 and S_2 by applying a whitening transformation derived from the eigenvector and eigenvalue factorization of the composite spatial covariance. As a result, $S_1$and

S_2 share common eigenvectors, and for a common eigenvector the summation of the eigenvalues is one. In other words, since we can write $S_1$and S_2 as

$$S_1 = V\Sigma_1 V^T \text{ and } S_2 = V\Sigma_2 V^T \quad (26)$$

then, $\Sigma_1 + \Sigma_2 = I$, where I is the identity matrix, V is the matrix of eigenvectors, and Σ_1 and Σ_2 are the diagonal matrices of eigenvalues for the two classes.

Hence, the eigenvector that corresponds to the largest eigenvalue for one group also corresponds to the smallest eigenvalue for the second group. Therefore, for classification purposes the EEG signals are typically projected onto the first and last columns of the projection matrix W of spatial filters defined as

$$\mathrm{W} = \mathrm{P}^T V \quad (27)$$

where P is the whitening transformation and can be written as

$$P = \sqrt{\lambda^{-1}} U^T \quad (28)$$

where U is the matrix of eigenvectors of the composite spatial covariance matrix C_c. Since EEG signals are nonstationary, we only consider samples after the cue.

3.7 Methods and Results

In this thesis, the goal is two folds. First, we would like to design favorable dictionaries that provide efficient sparse representation of EEG signals. Second, we use these representations to efficiently classify the motor imagery data. By obtaining the sparse representation of the signals, the class of the test trials can be determined by finding the *m*th residual defined in (10). The residual is the error between the test trials and the signal reconstructed by few atoms from the mth subdictionary. The class of x can be determined as the one with the minimal residual using (11).

Dataset 3a, and *Dataset 4a* are used in this work to evaluate the performance of the proposed algorithms. As previously discussed, *database3a* is a 4-class EEG database, recorded using 60 channels and 90 trials per class. These signals were checked by experts for artifacts and thus the marked trials were removed from experiment. Before using all four classes, the classification is performed using only two classes at a time.

The performance of the proposed methods is evaluated using a 4-fold cross validation. In this method, 75 % of the dataset is selected randomly as the training set and the remaining 25 % of

the data is considered as the test set. This procedure is repeated ten times to find a more realistic Correct Classification Percentage (CCP). The number of training examples from each class is fixed since having unequal number of columns from each class can degrade the sparse representation of the signals. The total number of trials for each class in *dataset3a* is shown in Table 1 after removing the marked trials.

Table 1 Number of trials in training and test sets for each class.

Dataset3a	Class 1	Class 2	Class 3	Class 4
Total number of trials	74	75	75	74
Training set	56	56	56	56
Test set	18	19	19	18

Each trial in *dataset3a* is a 60×1000 matrix, because 60 electrodes are used to record the signals and the used sampling frequency is 250 Hz. In *dataset4a*, the dimension of the trials is 118×350 since signals are downsampled to 100 Hz. An example of an Epoch from *dataset4a* is shown in Figure 16. This figure was produced using the EEGLAB toolbox [**32**].

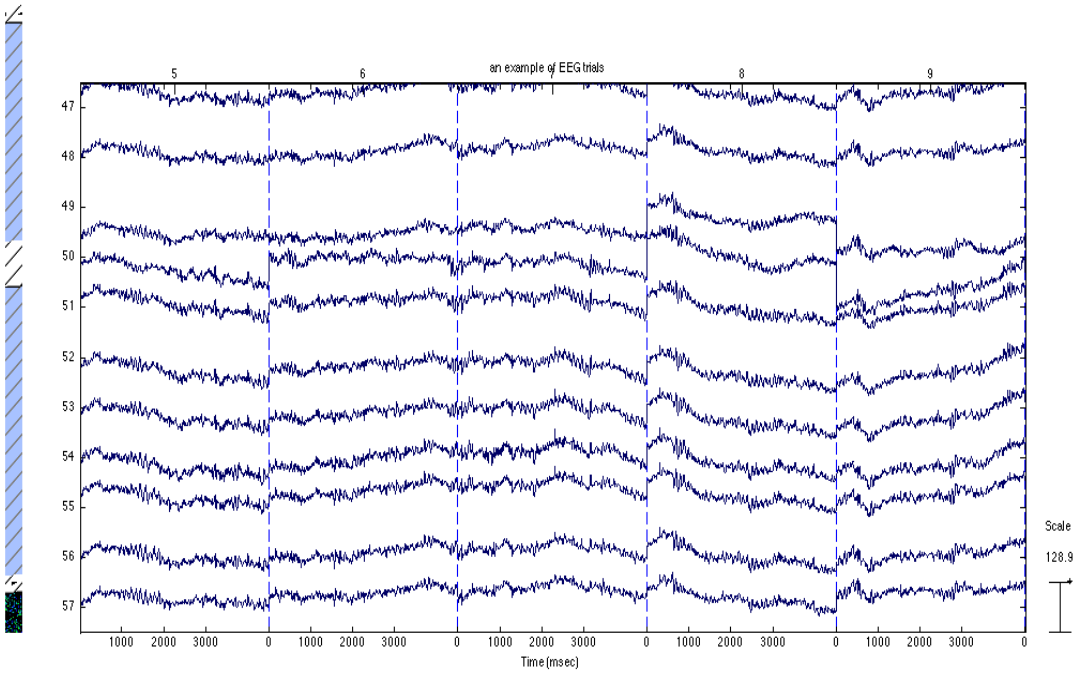

Figure 16 An example of EEG trials recorded with 10 channels including C3 position electrode (# 52).

Dataset4a consists of signals related to five healthy subjects, each with 280 trials. Since 25 percent of the signals are randomly selected, the test set contains 70 trials and the training set comprises 210 epochs in every iteration.

At the first step, trials recorded by all available electrodes (i.e. 60 in dataset3a and 118 in dataset 4a) are employed to obtain the spatial filters. Second, to support real time BCI, the electrodes are reduced to thirty for both datasets and the spatial filters are computed using the thirty electrodes.

These set of electrodes are selected since they are located close to the sensorimotor cortex. To further reduce the number of electrodes, the electrode position *C3* and four neighboring electrodes close to the sensorimotor cortex are used to obtain the spatial filters.

In this thesis only the spatial filter corresponding to the largest eigenvalue is used in most of the approaches. By obtaining the spatial filter, the EEG training signals from each class are projected on this spatial direction and then feature vectors are extracted and used to populate the columns of a subdictionary. These subdictionaries are concatenated to form our final multi-class dictionary. To this end, feature vectors based on the wavelet characteristics of the projected EEG signals are obtained.

Time-Frequency Analysis such as Discrete Wavelet Transforms (DWT) and Wavelet Packet Transforms (WPT) are two promising techniques in biomedical signal processing, particularly EEGs. Using time-frequency methods for non-stationary signals such as EEGs can improve the performance of the classification techniques. Building a dictionary based on wavelets can provide better frequency resolution. WPT and DWT can be best described using a filter bank approach, whereby signals are decomposed using a high pass filter $h[\,.\,]$ and a low pass filter $g[\,.\,]$ in each level of decomposition [**33**] .In contrast to the Discrete Wavelet Transform in which the decomposition of the signals continues only at the low frequency levels, in WPT the decomposition continues in both the high and low frequency sub-bands. The number of decomposition levels may vary based on the frequency characteristics of the signals. A wavelet

decomposition and also wavelet packet decomposition patterns are shown in Figure 17 and Figure 18 respectively.

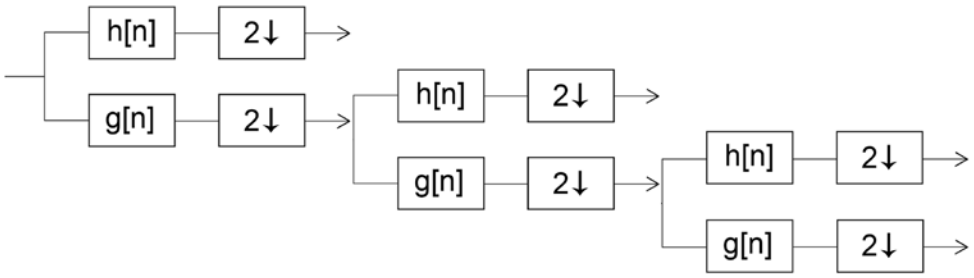

Figure 17 Discrete Wavelet decomposition in three levels using filterbank approach.

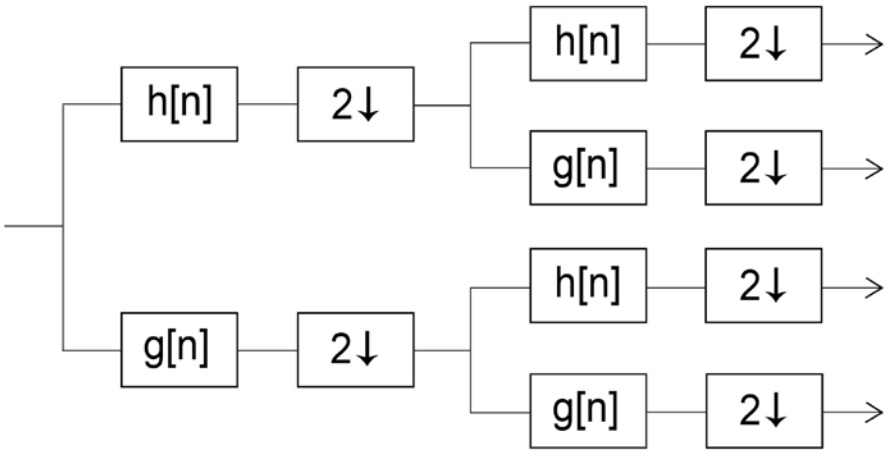

Figure 18 Wavelet Packet Transform is shown using filterbank approach.

In the first approach, a Daubechies-4 wavelet family is employed in four decomposition levels to obtain the wavelet coefficients of the Projected EEG trials. The wavelet coefficients generate the columns of the dictionary. In this approach, eight spatial filters corresponding to the four largest

and smallest eigenvalues are selected and the performance of the algorithm is evaluated using these filters individually. To reduce the dimension of the data, the wavelet coefficients in each frequency sub-bands are employed and the best results are presented. The block-diagram of this method is provided in Figure 19.

In Table 2 and Table 3 results for *dataset3a* and *dataset4a* are shown, respectively. In these tables, results related to the best frequency sub-bands for each subject or classes are reported.

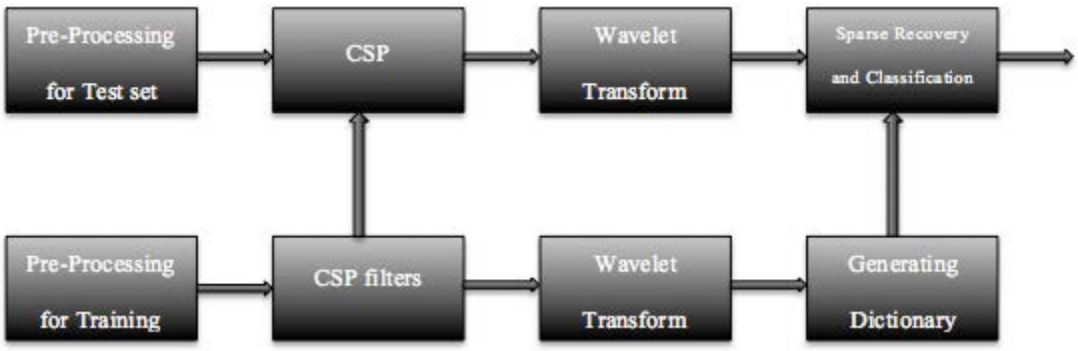

Figure 19 The block diagram of classification based on sparse representation of wavelet coefficients related to the EEG trials.

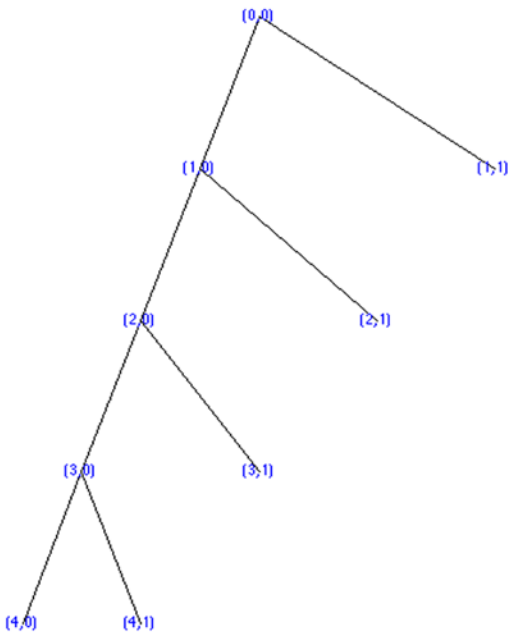

Figure 20 Discrete wavelet decomposition in 4 levels. Coefficients in different frequency sub-bands are used to find the sparse representation of the EEG trials.

Table 2 Results obtained using wavelet coefficients of one of the spatial filters for dataset3a.

Frequency sub-band	1	2	3	4	5	6	7	8
CCP% Class1 Vs. 2	58.38	55.00	54.59	53.11	49.73	47.09	62.77	**69.99**
CCP% Class1 Vs. 3	**84.39**	75.68	66.89	62.91	50.95	60.00	77.50	76.35
CCP% Class1 Vs. 4	**90.28**	77.01	71.81	65.90	52.71	53.96	54.65	54.31
CCP% Class2 Vs. 3	**89.41**	70.59	69.41	55.13	56.25	60.53	75.59	**82.70**
CCP% Class2 Vs. 4	55.54	57.09	48.18	51.62	66.01	74.80	69.12	**93.92**
CCP% Class3 Vs. 4	58.51	49.05	51.01	50.95	52.84	66.89	79.73	**82.77**

Table 3 Results based on the wavelet coefficients of individual spatial filters for dataset4a.

Frequency sub-band	1	2	3	4	5	6	7	8
Subject 1	51.36	50.64	51.79	51.14	50.61	50.64	50.36	52.79
Subject 2	**79.61**	**81.21**	**81.50**	78.43	52.00	51.35	49.55	54.34
Subject 3	**60.50**	54.71	52.79	54.29	49.73	49.14	51.14	51.86
Subject 4	77.86	74.82	75.21	77.61	**82.32**	**82.25**	**82.25**	**80.79**
Subject 5	**88.68**	74.93	75.00	71.14	69.14	70.46	70.89	72.39

As expected, results related to the first or last spatial filters appear to be the best in *dataset3a*. Table 2 shows promising classification results for most of the cases. Table 3 shows the results for *dataset4a*. It is observed that good classification performance is achieved for 3 subjects and the results are consistent.

In the second approach, we used the energy in the frequency sub-bands depicted in Figure 20 instead of the wavelet coefficients. Figure 21 shows the diagram for the proposed method.

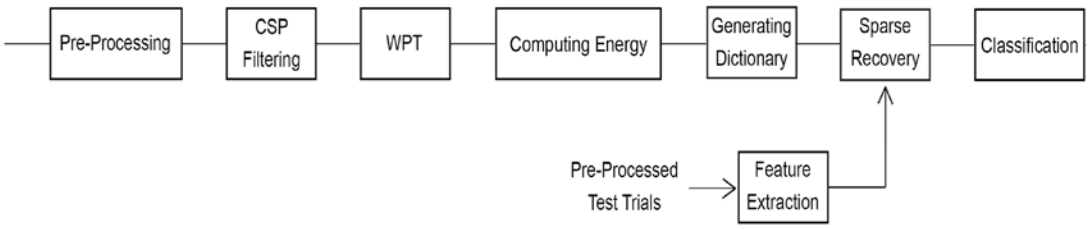

Figure 21 Block diagram of the energy-based feature vectors to find the sparse representation.

Let Y denote the $N \times Q$ EEG signal. After CSP an $M \times Q$ matrix is obtained, where N is the number of channels in the original EEG and M is the number of spatial filters in the CSP algorithm. In this approach, only one of the spatial filters corresponding to the largest or smallest eigenvalues is employed. As a result, one energy value is obtained at the lowest frequency sub-band called the approximation level, and L energy values are obtained in higher frequency sub-bands, where L is the number of decomposition levels. In this approach, the feature extraction step proceeds as follows

$$\begin{bmatrix} y_1^1 & y_2^1 & \dots & y_Q^1 \\ \vdots & & & \\ y_1^N & y_2^N & \dots & y_Q^N \end{bmatrix} \xrightarrow{CSP} [z_1 \quad \dots \quad z_Q] \xrightarrow{wavelet\ coef\ energy} \left[x_1^{apx} \quad x_1^d \quad \dots \quad x_L^d\right] \qquad (29)$$

Where x_1^{apx} is the energy entry for the approximation level and x_L^d are the energy entries in the detail levels. In this thesis the trials are decomposed in four levels. Therefore, a $5 \times (T \times$

N_c) dictionary is developed where T is the number of trials in each class and N_c the number of classes. Results are provided in Table 4 and Table 5 for *dataset3a* and *dataset4a*, respectively.

Table 4 Results for single sparsity of energies related to the five frequency sub-bands (dataset3a).

Class1 Vs. Class2	Class1 Vs. Class3	Class1 Vs. Class4	Class2 Vs. Class3	Class2 Vs. Class4	Class3 Vs. Class4
55.88	82.57	88.68	83.62	54.73	61.62

Table 5 Results for dataset4a using energies in five frequency sub-bands.

Subject 1	Subject 2	Subject 3	Subject 4	Subject 5
70.46	86.82	57.61	82.39	62.64

In the third approach, the energies in different frequency sub-bands are considered individually. For instance, only the energy entry related to the approximation level is used. To generate a vector of energies, all the eight spatial filters are employed instead of using only one of them. The EEGs are projected on the spatial filters. Then the energy values in a particular frequency sub-band can be obtained for all the projected EEGs. Concatenating the energy values, an $M \times 1$ vector is obtained that represents the EEG trial. The idea of concatenating energies obtained by employing all the spatial filters, was proposed in [**7**] .The results are provided in Table 6 and Table 7 for *dataset-3a and dataset-4a,* respectively.

Table 6 Results (CCP%) based on energies in one of the frequency sub-bands for dataset3a.

	Approximation level	Detail-01	Detail-02	Detail-03	Detail-04
Class1 Vs. 2	66.49	63.11	66.35	**67.91**	64.93
Class1 Vs. 3	95.54	86.15	**95.61**	**96.96**	90.27
Class1 Vs. 4	**91.33**	82.01	88.26	**90.80**	86.39
Class2 Vs. 3	93.16	83.22	92.50	**94.74**	90.39
Class2 Vs. 4	**88.51**	76.55	80.47	**85.20**	85.14
Class3 Vs. 4	88.24	76.89	**89.66**	**90.95**	78.72

Table 7 Results (CCP%) based on the energies of one of the frequency sub-bands for dataset4a.

Frequency sub-band	Approximation level	Detail-01	Detail-02	Detail-03	Detail-04
Subject 1	52.61	51.25	58.46	50.96	63.93
Subject 2	70.36	86.68	**89.50**	63.64	72.82
Subject 3	55.50	52.50	54.25	53.46	54.75
Subject 4	60.57	**88.43**	85.04	53.29	73.46
Subject 5	63.61	55.64	58.18	63.50	56.04

3.8 M-Class problem

Dataset3a gives us the opportunity to test the sparsity approach on multiple classes. CSP is a projection method whereby the dimension of the trials reduces significantly and also makes the data more separable but it works in two class problems. For multiple class problems an algorithm is introduced in [**34**], called One Versus the Rest CSP (OVR). In this method, to obtain the

spatial filters, one class is considered as one group and the remaining classes together form the other group. Solving the binary CSP, the spatial filters for that particular class are obtained. The OVR continues for all of the classes to find the spatial filters for each class.

EEG trials are projected using one of the spatial filters. The wavelet coefficients of the projected EEG trials are extracted and classification is done using the set of coefficients. The results are reported in Table 8.

Table 8 Classification of 4 classes using wavelet coefficients (dataset3a).

Frequency sub-band	Approximation level	Detail-01	Detail-02
CCP%	42.06	39.97	38.14

In M-class problems, using only one of the spatial filters cannot improve the results. The reason is that the spatial filter is obtained to increase the separability of one class versus all the rest, so the separability of other groups is not considered. To enhance the algorithm, we used all of the eight spatial filters. To this end, energies related to each frequency sub-bands are obtained. A vector of 5×1 is derived for each of the spatial filters. Concatenating them, a 40×1 vector represents the feature vector. Results are shown in Table 9.

Table 9 Classification of 4 classes using Wavelet coefficients energy.

Frequency sub-band	One Spatial Filter	All spatial Filters
CCP%	36.49	63.89

Based on the results from Table 9 it can be concluded that, using all the spatial filters in M-class problems is necessary to enhance the performance of classification. Using less data can decrease the computational complexity and can support real time BCI. Furthermore, execution and imagination of movement change the neuronal population activity over the sensorimotor areas. Therefore, instead of using all the channels, those near to the sensorimotor cortex are used. The position of the selected electrodes near the sensorimotor cortex is shown in Figure 22.

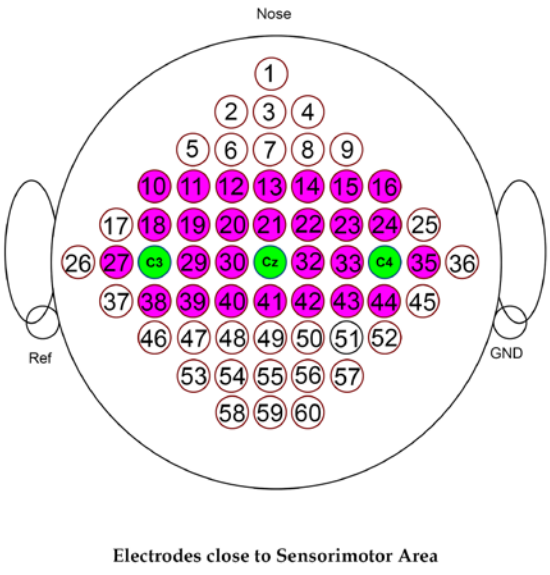

Figure 22 Thirty electrode close to the sensorimotor cortex are selected. This illustration belongs to dataset3a.

Instead of employing all 60 electrodes, only thirty electrodes near the sensorimotor cortex are used to obtain spatial filters (Figure 22). To classify the signals the sparse representation of the projected trials are obtained. Also, thirty electrodes are selected near the sensorimotor area in *dataset4a* to test the accuracy of the methods. The selected electrodes are shown in Figure 23. Table 10 and Table 11 show the results for using thirty electrodes.

Table 10 dataset3a results using thirty electrodes.

Methods	CCP
Wavelet Coefficients	40.24
Wavelet Coefficients Energy	63.41

Table 11 Dataset4a results obtained using thirty electrodes.

Sparse representation	Energy obtained using wavelet decomposition	Wavelet coefficients
Subject 1	68.43	71.11
Subject 2	86.93	87.39
Subject 3	57.11	63.18
Subject 4	74.96	76.00
Subject 5	64.21	74.07

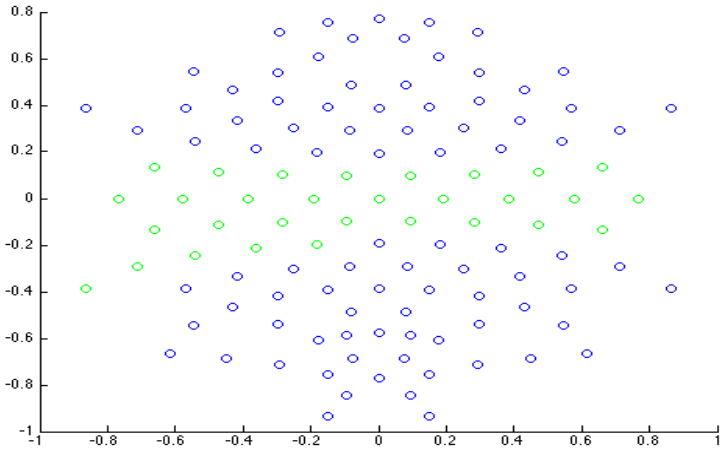

Figure 23 Thirty electrodes selected in dataset4a near the sensorimotor cortex.

3.9 Joint Sparsity Structure

Leveraging the correlation between neighboring electrodes is the motivation for finding the joint sparse representation. But avoiding the CSP algorithm to use the original EEG signals, deteriorate the classification performance. The joint sparsity structure is not preserved if the signals are projected along different spatial directions. Therefore jointly measurements are derived using one of the spatial filters.

We proposed two approaches to generate the dictionary. First, the five central electrodes including *C3* and four neighboring electrodes are projected along the spatial filter direction. Similar to the previous methods, wavelet coefficients can be obtained to generate the columns of the dictionary.

In the second approach, we generate the columns of the dictionary using a linear combination of all five neighborhoods around the *C3* electrode (Figure 24). As a matter of fact, all the colored electrodes in Figure 24 are involved, but the weight of the electrodes increases, as we get closer to the center *C3* because close neighborhoods share common electrodes.

In the Left Hand Side (LHS) of equation (3), instead of using one measurement, we need T vectors to be able to find the joint sparse representation of the measurements. To this end, T neighborhoods across the *C3* are projected along the spatial filter and then wavelet coefficients are computed. As a result a $B \times T$ matrix is generated in the LHS of (3), where each column represents one of the neighborhoods. Classification results of EEGs using joint sparse representation are shown in Table 12.

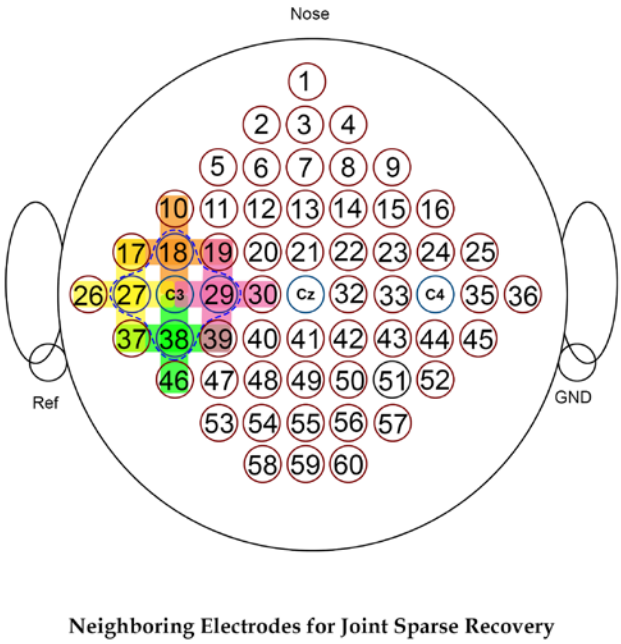

Figure 24 Central neighborhood and four close neighborhoods are selected for joint sparse recovery.

Table 12 Results for Joint sparse representation.

	Joint sparsity *C3* electrode	Joint sparsity Linear-comb	Single sparsity
Subject-1	60.82	60.36	59.75
Subject-2	71.11	74.93	85.93
Subject-3	57.36	59.04	56.39
Subject-4	74.36	77.43	76.96
Subject-5	61.93	60.57	68.07

3.10 Energy and Entropy

Using only five electrodes near the sensorimotor cortex makes the classification more challenging. Our approach for feature extraction is motivated by the aforementioned fact that there exist different levels within the alpha band carrying movement-specific patterns [**11**] that could potentially be captured through the energies, as well as their distribution in different frequency sub-bands.

The energies in different frequency sub-bands are computed using DWT and WPT. Employing WPT, the energy is computed in $L = 2^n$ frequency sub-bands to generate feature vectors for the EEG trials in $\mathbb{R}^L$, where n is the level of decomposition. In the second approach, we obtain feature vectors using the energy and the entropy of the signals. In particular, we append the entropy of the signals computed using the wavelet coefficients to the energy vectors. In this case, the features vectors are in $\mathbb{R}^{L+1}$.

The entropy of a signal z is calculated from the wavelet coefficients, using

$$Entropy(z) = -\sum_i s_i^2 \log s_i^2 \qquad (30)$$

where s_i is the i-th wavelet coefficient of z obtained from WPT. In the third approach, we generate the feature vectors directly from the wavelet coefficients.

The electrode position *C3* and four neighboring electrodes close to the sensorimotor cortex are used to obtain the spatial filters as shown Figure 25. We only use the spatial filter corresponding to the largest eigenvalue. The EEG training signals from each class are projected along this spatial direction and then the aforementioned feature vectors are extracted and used to populate the columns of a subdictionary. These subdictionaries are concatenated to form our final multi-class dictionary. Figure 26 shows the block diagram of this method.

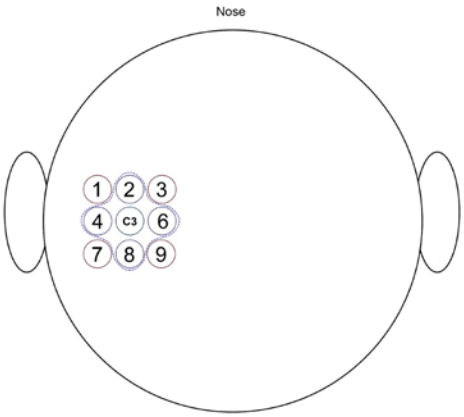

Figure 25 C3 and its four neighboring electrodes.

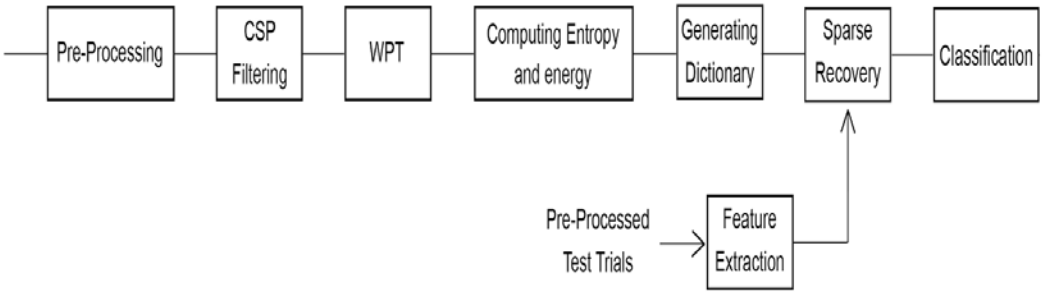

Figure 26 Block Diagram of the proposed classification algorithm based on sparse representation.

Results for this set of electrodes are reported in Table 13 and Table 14 for *dataset4a* and *dataset3a* respectively. Since *dataset3a* is an M-class problem, it was necessary to use all spatial filters; therefore the entropy and energy feature vectors related to spatial filters are concatenated to find the corresponding sparse representation. Figure 27 illustrates the wavelet packet decomposition into four levels and the frequency sub-bands wherein the energies are computed.

The proposed method in **[7]** is also simulated using the same set of electrodes and the results are provided in Table 15. In **[7]** power of the projected EEG trials are computed and then the power values are concatenated to form an $M \times 1$ vector where M is the number of spatial filters. Since there are only five electrodes, the number of spatial filters is four. Moreover, SVM as a well-known binary classifier is employed to classify the signals based on the extracted feature vectors. Results are provided in Table 16.

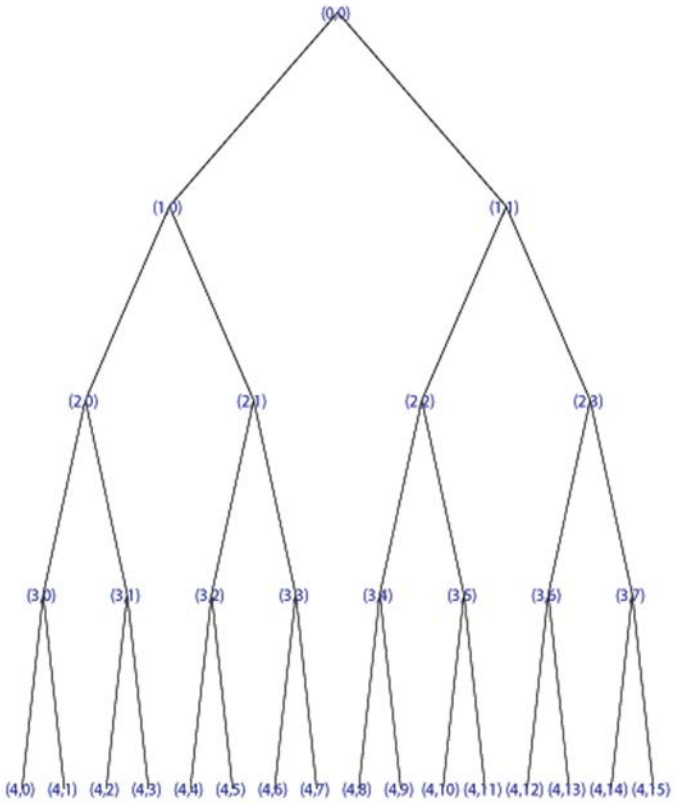

Figure 27 Wavelet Packet decomposition in four levels.

Table 13 Classification is done based on the sparse representation of the energy features and entropy.

Sparse representation	Energy obtained using wavelet decomposition	Energy obtained using wavelet packet	Energy and entropy concatenated
Subject 1	62.46	**64.79**	64.71
Subject 2	86.29	85.50	**89.71**
Subject 3	57.75	61.50	**64.25**
Subject 4	73.96	73.11	**93.07**
Subject 5	61.98	59.36	**83.71**

Table 14 Results for dataset3a classification, based on Sparse Representation where energy and entropy are extracted.

Methods	Energy obtained using wavelet decomposition	Energy obtained using wavelet packet	Energy and entropy concatenated
Dataset3a	43.07	39.70	**58.28**

Table 15 Results for method in **[7]**.

Subject 1	Subject 2	Subject 3	Subject 4	Subject 5
57.29	87.25	60.14	75.07	83.43

Table 16 Support Vector Machine is employed to classify the EEG trials.

SVM	Energy obtained using wavelet decomposition	Energy obtained using wavelet packet	Entropy	Energy and entropy concatenated
Subject 1	75.00	74.64	67.82	**76.93**
Subject 2	91.89	93.86	91.07	**95.54**
Subject 3	67.71	67.11	66.54	66.21
Subject 4	82.54	88.00	85.71	**96.29**
Subject 5	73.64	81.43	88.28	**89.32**

CHAPTER 4. SUMMARY AND CONCLUSION

In this work, an algorithm to classify motor imagery EEG signals to support real-time BCI was proposed. First, all the available electrodes are used to classify the signals. Then, dimensionality is reduced by selecting only thirty and then five significant electrodes near the sensorimotor cortex out of 118 available electrodes in *dataset4a* and 60 electrodes in *dataset3a*. Then, we leverage the sparse representation of the EEG trials in a multi-class dictionary learned from the wavelet characteristics of the signals.

Different feature vectors are extracted based on the wavelet coefficients, energies in different frequency sub-bands of the Wavelet Packet Decomposition or Discrete Wavelet Decomposition and the signal entropy. The results obtained from real data demonstrate that the combination of energy and entropy features enables efficient classification of motor imagery EEG trials related to hand and foot movement. This underscores the relevance of the energies and their distribution in different frequency sub-bands for classifying movement- specific EEG patterns in agreement with the existence of different levels within the alpha band.

Based on our results, it is seen that using thirty electrodes near the sensorimotor cortex does not degrade the performance in comparison to using all of the electrodes, yet leads to significant dimensionality reduction to support real-time BCI. Furthermore, it is possible to extend the dictionary-based classification method to M-class problems by concatenating the new training

sets related to new classes into the dictionary. Results for *Dataset3a* demonstrate that the combination of energy and entropy can enhance the classification of motor imagery EEG signals in M-class problems. Although the number of electrodes is reduced from 60 to 5, considering the energies and their distribution could preserve the separability among the four classes.

Future work will focus on more refined models to exploit the spatial correlation, and will investigate techniques that are robust to noise. Another direction of future research will explore similar sparse representation in other brain signal classification problems such as epilepsy.

LIST OF REFERENCES

[1] T. W. Berger, J. K. Chapin, G. A. Gerhardt, D. J. McFarland, J. C. Principe, W. V. Soussou, D. M. Taylor and P. A. Tresco, *An international assessment of research and development trends*.: Springer Netherlands, 2008.

[2] W. F. Ganong and K. E. Barrett, *Review of medical physiology*. New york: New York: McGraw-Hill Medical, 2005, vol. 21.

[3] J. E. Hall, *Guyton and Hall textbook of medical physiology*.: Elsevier Health Sciences, 2010.

[4] J. Webster, *Medical instrumentation: application and design*.: John Wiley & Sons, 2009.

[5] E. J. Candès and M. B. Wakin, "An introduction to compressive sampling.," *IEEE Signal Processing Magazine*, vol. 25, no. 2, pp. 21-30, 2008.

[6] C. Yi, N. M. Nasrabadi and T. D. Tran, "Hyperspectral image classification using dictionary-based sparse representation," *IEEE Transactions on Geoscience and Remote Sensing*, vol. 49, no. 10, pp. 3973-3985, 2011.

[7] Y. Shin, S. Lee, J. Lee, and H. N. Lee, "Sparse representation-based classification scheme for motor imagery-based brain–computer interface systems," *Journal of neural engineering*, vol. 9, no. 5, p. 056002, 2012.

[8] A. Subasi, and M. I. Gursoy, "EEG signal classification using PCA, ICA, LDA and

support vector machines," *Expert Systems with Applications*, vol. 37, no. 12, pp. 8659-8666, 2010.

[9] H. Ocak, "Automatic detection of epileptic seizures in EEG using discrete wavelet transform and approximate entropy," *Expert Systems with Applications*, vol. 36, no. 2, pp. 2027-2036, 2009.

[10] P. L. Nunez, and R. Srinivasan, *Electric fields of the brain: the neurophysics of EEG*.: Oxford university press, 2006.

[11] G. Pfurtscheller, "Induced oscillations in the alpha band: functional meaning," *Epilepsia*, vol. 44, no. s12, pp. 2-8, 2003.

[12] G. Pfurtscheller, C. Brunner, A. Schlögl, and F. L. D. Silva, "Mu rhythm (de) synchronization and EEG single-trial classification of different motor imagery tasks," *Neuroimage*, vol. 31, no. 5, pp. 153-159, 2006.

[13] G. Pfurtscheller, and D. F. L. Silva, "Event-related EEG/MEG synchronization and desynchronization: basic principles," *Clinical neurophysiology*, vol. 110, no. 11, pp. 1842-1857, 1999.

[14] G. Pfurtscheller, and A. Aranibar, "Event-related cortical desynchronization detected by power measurements of scalp EEG," *Electroencephalography and clinical neurophysiology*, vol. 42, no. 6, pp. 817-826, 1977.

[15] G. Pfurtscheller, "the cortical activation model (CAM)," in *Progress in Brain Research-Event-Related Dynamics of Brain Oscillations*, Christa Neuper &

Wolfgang Kimesch, Ed.: Elsevier, 2006, vol. 159, pp. 19-27.

[16] G. Pfurtscheller, and C. Neuper, "Motor imagery activates primary sensorimotor area in humans," *Neuroscience letters*, vol. 239, no. 2, pp. 65-68, 1997.

[17] G. Pfurtscheller and C. Neuper, "Event-related synchronization of mu rhythm in the EEG over the cortical hand area in man," *Neuroscience letters*, vol. 174, no. 1, pp. 93-96, 1994.

[18] B. Blankertz, R. Tomioka, S. Lemm, M. Kawanabe and K. R. Muller, "Optimizing spatial filters for robust EEG single-trial analysis," *IEEE Signal Processing Magazine*, vol. 25, no. 1, pp. 41-56, 2008.

[19] Y. Wang, S. Gao and X. Gao, "Common spatial pattern method for channel selelction in motor imagery based brain-computer interface," in *27th Annual International Conference of the Engineering in Medicine and Biology Society IEEE-EMBS*, 2005, pp. 5392-5395.

[20] D. L. Donoho, "Compressed sensing," *IEEE Transactions onInformation Theory*, vol. 52, no. 4, pp. 1289-1306, 2006.

[21] E. J. Candès, J. Romberg and T. Tao, "Robust uncertainty principles: Exact signal reconstruction from highly incomplete frequency information. ," *Information Theory, IEEE Transactions*, vol. 52, no. 2, pp. 489-509, 2006.

[22] R. G. Baraniuk, "Compressive sensing," *IEEE signal processing magazine*, vol. 24, no. 4, 2007.

[23] J. A. Tropp and A. C. Gilbert, "IEEE Transactions on Information Theory," *Signal recovery from random measurements via orthogonal matching pursuit.*, vol. 53, no. 12, pp. 4655-4666, 2007.

[24] J. A. Tropp, A. C. Gilbert and M. J. Strauss, "Algorithms for simultaneous sparse approximation. Part I: Greedy pursuit," *Signal Processing*, vol. 86, no. 3, pp. 572-588, 2006.

[25] R. Boostani, B. Graimann, M. H. Moradi and G. Pfurtscheller, "A comparison approach toward finding the best feature and classifier in cue-based BCI.," *Medical & biological engineering & computing*, vol. 45, no. 4, pp. 403-412, 2007.

[26] G. Garcia, T. Ebrahimi and J. Vesin, "Support Vector EEG Classification in the Fourier and Time-Frequency Correlation," in *In Proceedings of the IEEE-EMBS First International Conference on Neural Engineering*, 2003, pp. 591-594.

[27] A. Schlögl and G. Pfurtscheller, BCI competition. [Online]. http://www.bbci.de/competition/iii/desc_IIIa.pdf

[28] B. Blankertz, Berlin brin-computer interface. [Online]. http://www.bbci.de/competition/iii/desc_IVa.html

[29] H. Ramoser, J. Muller-Gerking, and G. Pfurtscheller, "Optimal spatial filtering of single trial EEG during imagined hand movement," *IEEE Transactions on Rehabilitation Engineering*, vol. 8, no. 4, pp. 441-446., 2000.

[30] Z. J. Koles, M. S. Lazar, and S. Z. Zhou, "Spatial patterns underlying population

differences in the background EEG.," *Brain topography*, vol. 2, no. 4, pp. 275-284, 1990.

[31] J. Müller-Gerking, G. Pfurtscheller, and H. Flyvbjerg, "Designing optimal spatial filters for single-trial EEG classification in a movement task," *Clinical neurophysiology*, vol. 110, no. 5, pp. 787-798, 1999.

[32] A Delorme and S Makeig., "EEGLAB: an open source toolbox for analysis of single-trial EEG dynamics," *Journal of Neuroscience Methods*, vol. 134, pp. 9-21.

[33] S. Mallat, *A wavelet tour of signal processing.*: Academic press, 1999.

[34] G. Dornhege, B. Blankertz, G. Curio, and K. R. Müller, "Boosting bit rates in noninvasive EEG single-trial classifications by feature combination and multiclass paradigms," *EEE Transactions on Biomedical Engineering*, vol. 51, no. 6, pp. 993-1002, 2004.